Applied Catalysis B: Environmental 140–141 (2013) 249–257

Contents lists available at SciVerse ScienceDirect

Applied Catalysis B: Environmental

journal homepage: www.elsevier.com/locate/apcatb

Microstructured Au/Ni-fiber catalyst for low-temperature gas-phase alcohol oxidation: Evidence of Ni_2O_3–Au^+ hybrid active sites

Guofeng Zhao [a], Jun Huang [b], Zheng Jiang [c], Shuo Zhang [c], Li Chen [a], Yong Lu [a,*]

[a] Shanghai Key Laboratory of Green Chemistry and Chemical Processes, Department of Chemistry, East China Normal University, Shanghai 200062, China
[b] School of Chemical and Biomolecular Engineering, University of Sydney, NSW 2006, Australia
[c] Shanghai Synchrotron Radiation Facility, Shanghai Institute of Applied Physics, Chinese Academy of Sciences, Shanghai 201204, China

ARTICLE INFO

Article history:
Received 12 February 2013
Received in revised form 21 March 2013
Accepted 5 April 2013
Available online 11 April 2013

Keywords:
Gold catalyst
Alcohol oxidation
Nanostructure
Active site
Galvanic reaction

ABSTRACT

Microfirous-structured Au/Ni-fiber catalysts prepared by Au galvanic deposition method are active and selective for the gas-phase oxidation of alcohols. The nature of their excellent low-temperature activity is explored especially by means of X-ray photoelectron spectroscopy (XPS) and X-ray absorption near-edge structure (XANES). An interesting NiO@Au ensemble nanostructure (*i.e.*, partial coverage of Au particles with NiO segments) was clearly identified, which is governing the high low-temperature activity. XPS and XANES studies indicate that the NiO@Au ensembles provide a unique synergistic effect, inducing a high surface concentration of Ni_2O_3–Au^+ hybrid active sites. The Ni_2O_3 specimens not only promote the formation of Au^+ cations and stabilize them but also serve as active O species reservoir. It is also proposed that O_2 is activated on the oxygen vacancy of Ni_2O_3 and then the adsorbed O atoms spill over onto Au^+ cations to react with alcohols.

1. Introduction

In recent decades, gold catalysis has attracted growing interest in the field of chemistry and chemical engineering. Compared to the inactive bulk gold, the gold nanoparticles (Au NPs) highly dispersed on oxide supports become active and selective catalysts for reactions such as low-temperature CO oxidation, hydrogenation, propylene epoxidation, and alcohol oxidation [1–5]. The size of the Au NPs [2–9], the support properties [10–15], and the Au-support interactions [2–4] have been proposed to be critical for their outstanding catalytic activity. The Au NPs smaller than 5 nm, especially in the range of 2–3 nm, have proved to be catalytically active [4,6], which might be due to many uncoordinated gold atoms present on the small Au NPs. Nevertheless, the activity of such Au NPs is often sensitive to the support properties [10–15] such as type, morphology (shape), and size. For example, Corma and co-workers reported that gold catalyst supported on nanoparticulated CeO_2 exhibited very higher activity than that supported on regular particle size CeO_2 in CO [14] or alcohol [15] oxidation. In addition, the charge transfer between support and small Au NPs also contributes to the catalytic activity of gold catalyst [4].

Although the origin of the Au NP activity has been intensively discussed through the above aspects, all the studies were based on the small Au NPs (<5 nm). However, this fundamentally important issue is required to be reconsidered. Unlike the previous findings, some recent reports showed that the large gold NPs (>20 nm) also exhibited excellent catalytic activity in many reactions. For example, the Au/SiO_2 [16] and $Au–Cu/SiO_2$ [17] catalysts delivered high activity for the oxidation of alcohols on the large Au NPs of 20 nm. Very recently, we developed Au/Ni-fiber catalyst for the gas-phase oxidation of benzyl alcohol with a high conversion of ~94% at a low temperature of 250 °C on the Au NPs of 25–30 nm [18]. Particularly, the high catalytic activity was reached on the novel model catalysts compared to that on the corresponding partner nanocatalysts, *i.e.*, noble metals supported on oxides. These catalysts were prepared by depositing transition metal oxides on the single crystal of noble metals, such as $CeO_2/Au(1\,1\,1)$ [19], $TiO_2/Au(1\,1\,1)$ [19,20], and $FeO/Pt(1\,1\,1)$ [21,22]. However, the fundamental mechanisms associated with this activity on the large Au NPs have not been clearly discussed therein.

Reaction takes place on the active sites of catalyst. The nature of these active sites, including their local structure and surface composition, is essential to understand the origin of their catalytic activity. Several models have been proposed for the formation of active centers on various ensembles: (1) the corner-step active sites on Au/MO_x with Au NPs loaded on support [6,15,23]; (2) monoatom/cation of gold dispersed on CeO_2 [22] and Pd or Ni surface [24–27]; (3) alloy active sites on Au–Pd core–shell structure and Au–Ni alloy nanoparticles [28,29]; and reactive perimeter around Au NPs [20,30]. For $CeO_2/Au(1\,1\,1)$, $TiO_2/Au(1\,1\,1)$ and $FeO/Pt(1\,1\,1)$

* Corresponding author. Tel.: +86 21 62233424; fax: +86 21 62233424.
E-mail address: ylu@chem.ecnu.edu.cn (Y. Lu).

0926-3373/$ – see front matter © 2013 Elsevier B.V. All rights reserved.
http://dx.doi.org/10.1016/j.apcatb.2013.04.015

catalysts [19–22], the metal-oxide interface is crucial for the formation of active sites, and the cooperative effects at oxide-metal interfaces delivered the high catalytic activity during the reactions [19–22].

As reported in the previous work, gold on nickel fiber catalysts were successfully prepared by Au galvanic deposition method [18,31]. The catalysts have excellent heat conductivity and stability, and are highly active and selective in the gas-phase oxidation of alcohols, opening an opportunity to shift traditional methods based on toxic and expensive inorganic oxidants to greener and more atom-efficient selective oxidation processes [18,31]. It has been proposed that the enhancement of the low-temperature activity of the Au/Ni-fiber catalysts could be contributed to the appearance of NiO NPs in spite of large gold particle size (20–30 nm). The following details need to be further clarified: (1) Are the unique Au–NiO nanocomposites formed? (2) If so, what is the amplified image of the nanocomposite structure in the microscopic vision? (3) What synergistic effect is derived from the special nanocomposite structure and what is the reaction mechanism over there?

Herein, the morphology and nanostructure of the catalysts were investigated by transmission electron microscopy (TEM) and scanning electron microscopy (SEM), identifying an interesting NiO@Au ensemble nanostructure (*i.e.*, partially covered Au particles with NiO segments). Accordingly, a series of reference catalysts were evaluated in the gas-phase aerobic oxidation of benzyl alcohol, for clarifying the enhancing conversion on the NiO@Au ensemble catalysts. Temperature-programmed desorption (TPD) and *in situ* diffuse reflectance infrared Fourier transform spectroscopy (DRIFTS) for ethanol adsorption were used to detect the synergistic effect of NiO@Au ensembles anchored on Ni-fiber. Furthermore, X-ray absorption near-edge structure (XANES) and X-ray photoelectron spectroscopy (XPS) were used to characterize the samples for clear identification of the active sites in the NiO@Au ensemble nanostructure.

2. Experimental

2.1. Catalyst preparation and reactivity evaluation

The catalysts were labeled as Au-*x*/Ni-fiber-*y*, where "*x*" denotes Au loading and "*y*" denotes calcination temperatures. For example, the catalyst Au-4/Ni-fiber-300 with gold loading of 4 wt% was calcined at 300 °C in air.

For comparison study, Au-4@NiO/Ni-fiber-C-300, Au-4/Ti-fiber-300 and Au-4/Stainless-Steel-fiber-300 (denoted as Au-4/SS-fiber-300), were prepared by incipient impregnation method at room temperature. A nominal amount of aqueous $HAuCl_4$ solution was prepared for incipient impregnation on the corresponding sintered-fiber supports. The Au-4/Ni-fiber-W-300 catalyst was obtained by washing the as-prepared Au-4/Ni-fiber sample using deionized water before drying in order to remove the produced $NiCl_2$ from the galvanic reaction ($2HAuCl_4 + 3Ni = Au + 3NiCl_2 + 2HCl$). For Au-4@NiO/Ni-fiber-C-300 catalyst, sintered Ni-fiber substrate was calcined in air at 600 °C for 1 h to obtain NiO/Ni-fiber (denoted as NiO/Ni-fiber-C-300) prior to loading Au. All the resulting samples were dried at 80 °C overnight and calcined at 300 °C for 2 h in air to obtain the fresh samples. The Ti-fiber (16 μm dia.) was purchased from IntraMicron, Ltd. (USA), and stainless steel 316L fiber (8 μm dia.) was purchased from Western Metal Material Co., Ltd. (China).

Furthermore, NiO/Ni-fiber-300, NiO-4@Au-4/Ni-fiber-W-300, NiO-4@Ti-fiber-300, NiO-4@Au-4/Ti-fiber-300 and NiO-4@Au-4/SS-fiber-300 catalysts with post-added 4 wt% of NiO were also prepared for comparison, by incipiently impregnating the corresponding Ni-fiber, Au-4/Ni-fiber-W-300, Ti-fiber, Au-4/Ti-fiber-300 and Au-4/SS-fiber-300 samples with aqueous solution containing a nominal amount of $Ni(NO_3)_2{\cdot}6H_2O$ (Sinopharm Chemical Reagent Co. Ltd., China). It should be noted that Au-4/SS-fiber was thoroughly washed by deionized water to remove the produced $FeCl_x$ (from the reaction: $HAuCl_4 + Fe \rightarrow Au + FeCl_x$) before post NiO-doping. All the resulting samples were dried at 80 °C overnight and calcined at 300 °C for 2 h in air again.

All the catalyst samples were pre-activated (*i.e.*, catalysts underwent gas-phase selective oxidation of benzyl alcohol at 380 °C for 1 h using O_2/ol (molar ratio of O_2 to alcoholic hydroxyl) = 0.6 and WHSV = 20 h^{-1}), and then evaluated in the gas-phase aerobic oxidation of benzyl alcohol at the given temperature in a fixed-bed quartz tube reactor (*i.d.*, 16 mm) under ambient pressure as described elsewhere [18,31,32].

2.2. Catalyst characterizations

The catalyst samples were characterized by X-ray diffraction (XRD, Rigaku Uitima IV diffractometer, Cu Kα), SEM (Hitachi-S4800), TEM (JEOL-JEM-2010 at 200 kV), and TPD on Quantachrome ChemBET 3000 chemisorption apparatus with a thermal conductive detector (TCD) and an online mass spectrometer (Proline Dycor, AMETEK Process Instrument).

The *in situ* DRIFTS experiments were performed on a Nicolet Nexus 670 Fourier transform infrared spectroscopy (FTIR) spectrometer equipped with a liquid-nitrogen cooled mercury cadmium telluride (MCT) detector by taking 512 scans at a resolution of 4 cm^{-1}. A high-temperature DRIFTS reactor cell with ZnSe window (Nexus Smart Collector) that connected with a purging/adsorption gas control system was utilized for *in situ* ethanol adsorption measurements. Catalysts were packed into the sample vessel of the reactor cell and pretreated at 100 °C with helium (30 mL/min) for 1 h and then cooled to room temperature under helium purging, prior to adsorption experiments. For each trial, the spectrum taken at room temperature in helium was used as a background reference. Helium flow of 30 mL/min was switched to pass through a vapor saturator with ethanol that immersed in a water bath (25 °C) for ethanol feeding. After that, the spectra were recorded at programmed temperature from 50 to 300 °C in static atmosphere. The subsequent continuous *in situ* reaction was carried out in the ethanol/helium mixed stream at 200 °C for 2.5 h over the pre-activated Au-4/Ni-fiber-300 (Au-loading: 4 wt%; calcined at 300 °C in air), pre-activated Au-4/Ni-fiber-W-300 and pre-activated NiO-4/Ni-fiber-300.

X-ray photoelectron spectroscopy (XPS) were recorded on a VG EscaLab 220i spectrometer, using a standard Al Kα X-ray source (300 W) and an analyzer pass energy of 20 eV, with the base pressure during XPS analysis of about 5×10^{-9} Torr. XANES data of the Ni K-edge (8333 eV) and Au L^{III}-edge (11,919 eV) were collected in the transmission mode on the BL14W1 beamline of the Shanghai Synchrotron Radiation Facility (SSRF). The typical electron beam energy was 3.5 GeV, and the current was 300 mA. A cryogenically cooled double-crystal Si(1 1 1) monochromator was used to minimize the harmonics. The XANES spectra were analyzed by the ATHENA software. The experimental backscattering amplitude and phase shift for the Au–Au pair were extracted from the Au foil, and the theoretical parameters for the Au–O, Au–Au, Ni–O and Ni–Ni pairs were calculated using the FEFF8.20 code.

3. Results and discussion

3.1. Unique active NiO@Au ensembles

It has been reported that the supported Au NPs on NiO is highly active for some reactions, such as CO low-temperature oxidation [1] and alcohol selective oxidation [33]. The Au-support interactions were proposed to be important to the catalytic activity of these

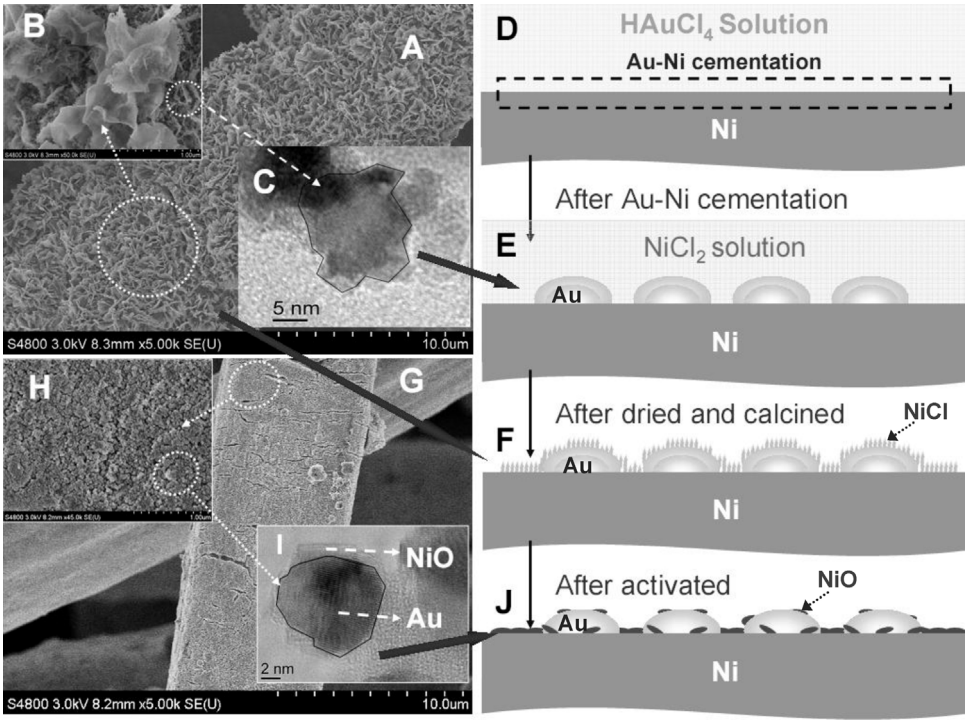

Fig. 1. Morphology and surface structure of the Au-4/Ni-fiber-300 catalyst. (A and B) SEM and (C) TEM images of the as-prepared Au-4/Ni-fiber-300; (D) The scheme of the Au–Ni galvanic exchange reaction; (E) The scheme of Au-4/Ni-fiber after galvanic exchange reaction; (F) The scheme of the fresh Au-4/Ni-fiber-300; (G and H) SEM and (I) TEM images of the pre-activated Au-4/Ni-fiber-300; (J) The scheme of the active NiO@Au ensembles over the pre-activated Au-4/Ni-fiber-300. Pre-activation conditions: The activated sample was obtained by being pre-activated at 380 °C for 1 h in reaction steam of benzyl alcohol with O_2/ol = 0.6 and WHSV = 20 h^{-1}.

catalysts, but such proposal was on the basis of small Au NPs. Very recently, a microfibrous-structured gold catalyst of Au/Ni-fiber was successfully developed with the aid of galvanic exchange reaction by our group. Interestingly, the Au/Ni-fiber catalyst is highly active, selective, and stable for the gas-phase oxidation of alcohols, although the gold particles are very large (25–30 nm) [18,31]. For example, the benzyl alcohol conversion of 95% was achieved with 99% selectivity to benzaldehyde within 660 h test at 250 °C over the Au-4/Ni-fiber catalyst (Au loading: 4 wt%), which is much better than other reported catalysts such as K–Cu–TiO_2 [34] and Au/Cu-fiber [35]. Our previous investigation showed that the transformation of $NiCl_2$ (formed at Au galvanic deposition step) into NiO was identified along with the low-temperature activity promotion [31]. This suggests a special synergistic effect between NiO and Au particles, of which comprehensive understanding is particularly desirable.

In heterogeneous catalysis, it is already recognized that the performance of a solid catalyst is determined mainly by its surface structure and composition. Identifying the active ensembles and discovering the active site on the Au/Ni-fiber catalyst is a crucial step in this research.

3.1.1. Formation of the $NiCl_2$@Au precursor

The Ni-fiber surface is composited of metallic Ni and NiO (Fig. S1). During catalyst preparation, the galvanic exchange reaction between $HAuCl_4$ solution and Ni-fiber took place and produced the metallic Au particles as well as $NiCl_2$. This process could be confirmed by XRD results, because diffraction patterns of $NiCl_2$ at 16.0° was observed over the dried Au-4/Ni-fiber catalyst precursor (Fig. S2). However, when the catalyst sample was washed thoroughly by deionized water just after undergoing the galvanic exchange reaction prior to drying and calcining, the XRD diffraction patterns of $NiCl_2$ disappeared rather than the Au XRD peak at 38.3°. SEM/EDX results could further confirmed the occurrence of such galvanic exchange reaction between $HAuCl_4$ solution and Ni-fiber (Figs. 1A, B and S3). As evidenced by XPS results (Figs. S1 and S4A, B), the surface of as-prepared catalyst contained $NiCl_2$ (dominant; Ni^{2+}: 856.5 eV) and NiO (Ni^{2+}: 854.4 eV), as well as metallic and cationic gold (metallic gold is dominant; Au^0: 83.8 eV, Au^I: 84.8 eV, Au^{III}: 86.2 eV [15,36]); no metallic Ni (852.5 eV) was detected, indicating that the Ni-fiber surface was completely covered with the gold and nickel species formed from the galvanic exchange reaction. As shown in the TEM images (Fig. 1C), the contrast level clearly exhibited that the gold particles seemed to have a lamellar ensembles consisting of multilayer and rough perimeter. This structure and morphology of the Au particles may be produced from the fast Au–Ni galvanic reaction.

It could be reasonably inferred from the above results that Au particles and $NiCl_2$ were produced from the $HAuCl_4$–Ni galvanic exchange reaction. As a result, Au particles were anchored firmly on the Ni-fiber surface and $NiCl_2$ was dissolved in water. In the process of drying at 80 °C, the $NiCl_2$ deposit was formed along with the fiber and partially covered the Au particles to form $NiCl_2$@Au composites (Figs. 1A, B, S1 and S4A, B). Fig. 1D–F schematically describes the $HAuCl_4$–Ni galvanic exchange reaction and the formation of active ensemble precursor of $NiCl_2$@Au.

3.1.2. Formation of active NiO@Au ensembles

Along with the pre-activation at 380 °C, the flower-like $NiCl_2$ (Fig. 1A and B) disappeared and the NiO particles were produced (Fig. 1G and H). That means the surface $NiCl_2$ was transformed into the NiO [18,31]. The XRD patterns demonstrate the main characteristic peaks of metallic nickel, metallic gold and NiO phase, with the disappearance of $NiCl_2$ in the pre-activated Au-4/Ni-fiber-300 catalyst (Fig. S5). The XPS spectra show that the catalyst surface was composed of Au^0 and Au^+, as well as NiO and Ni_2O_3 (the detailed analysis of Ni_2O_3 in Supporting information I) (Figs. S1 and S4C, D). No chlorine and metallic nickel were detected by XPS (Figs. S4C, D and S6), indicating that all the $NiCl_2$ was transformed into the NiO–Ni_2O_3 and the Ni-fiber surface was completely covered by Au

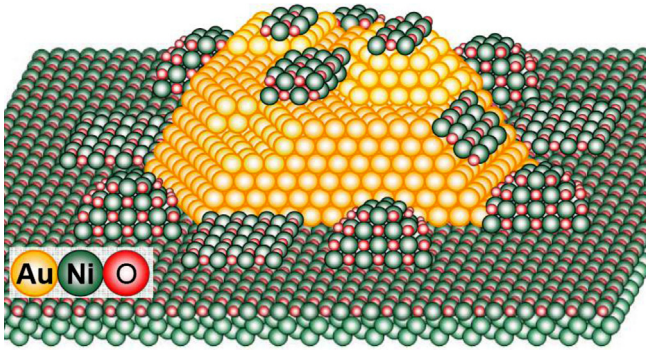

Fig. 2. The model of the partial coverage structure of the date-cake-like active NiO@Au ensembles of the pre-activated Au-4/Ni-fiber-300.

and NiO–Ni_2O_3. The TEM image in Fig. 1I shows a date-cake-like NiO@Au ensembles. The small NiO segments, like dates, partially covered the large gold particle, like a cake, to form the interesting active ensembles. Such unique ensemble structure was also confirmed by the coexistence of Au and NiO on the catalyst surface, as evidenced by the XPS results (Fig. S4C and D). A simple illustration is described in Fig. 1J and the detailed date-cake model for the NiO@Au ensembles is present in Fig. 2.

Therefore, the pre-activation of the as-prepared catalyst at 380 °C induced a surface reconstruction and the primary $NiCl_2$@Au precursor was converted to the active NiO@Au ensembles.

3.1.3. *Indispensability of the special NiO@Au ensembles*

The identified active NiO@Au ensembles (*i.e.*, with special structure of partial coverage of Au particles with NiO segments) on the pre-activated Au-4/Ni-fiber-300 exhibited an excellent catalytic activity, over which the benzyl alcohol conversion was 99% at 280 °C (Table 1: Au-4/Ni-fiber-300). For reference, neat Ni-fiber was tested and delivered a very low benzyl alcohol conversion of <2% with selectivity of 99% under identical reaction conditions (Table 1: Ni-fiber), indicating that the high benzyl alcohol conversion of 99% is attributed to NiO@Au ensembles.

Interestingly, when the as-prepared Au-4/Ni-fiber was washed to remove the $NiCl_2$ after galvanic exchange reaction prior to drying and calcining (*i.e.*, no NiO was obtained from $NiCl_2$ to partially cover Au particles), the benzyl alcohol conversion was only 39% (Table 1: Au-4/Ni-fiber-W-300). Only NiO supported on Ni-fiber offered a very low benzyl alcohol conversion of 5% (Table 1: NiO-4/Ni-fiber-300). However, after post-adding NiO to Au-4/Ni-fiber-W-300 to form the active ensembles of NiO@Au (Fig. S7A and B), the conversion of benzyl alcohol was greatly increased to 94% (Table 1: NiO-4@Au-4/Ni-fiber-W-300).

In addition, the Au-4/Ti-fiber-300 catalyst prepared by impregnation delivered an Au particle size of 27 nm, comparable to that of the Au-4/Ni-fiber-300 catalyst. This catalyst offered benzyl alcohol conversion of only 8% with 99% selectivity to benzaldehyde at 280 °C (Table 1: Au-4/Ti-fiber-300). Similarly, only NiO particles supported on Ti-fiber delivered a much lower conversion of 4% (Table 1: NiO-4/Ti-fiber-300) while the post NiO-doping (NiO-4@Au-4/Ti-fiber-300) remarkably promoted the activity with a benzyl alcohol conversion of 95% at 280 °C. In Fig. S7C and D, the TEM images of the NiO-4@Au-4/Ti-fiber-300 clearly show the formation of NiO@Au ensembles by the post NiO-doping Au-4/Ti-fiber-300 catalyst. It seems that the identified active NiO@Au ensembles over the pre-activated catalysts play an important role in exhibiting an excellent catalytic activity.

Whether is the special structure indispensable, or is there any other ensembles, such as Au@NiO (NiO partially covered with Au particles) or MO_x@Au particles (Au particles partially covered with other metal oxides), also contributing an excellent catalytic activity? On the Au-4@NiO/Ni-fiber-C-300, the maximum conversion of 39% with 99% selectivity could be obtained in the selective oxidation of benzyl alcohol (Table 1 and Supporting information II). Similar to the Au-4/Ni-fiber-300, the Au-4/SS-fiber-300 was prepared by the galvanic reaction occurring between SS-fiber and $HAuAl_4$. The FeO_x@Au ensembles delivered an almost comparable Au particle size (23 nm) but induced a benzyl alcohol conversion of only 17% with 99% selectivity even at 280 °C (Table 1: Au-4/SS-fiber-300). However, replacing FeO_x with NiO (denoted as NiO-4@Au-4/SS-fiber-300) remarkably promoted the benzyl alcohol conversion to 89%, similar with the NiO-4@Au-4/Ti-fiber-300. One thus can say that the NiO@Au ensembles are definitely contributed to the excellent low-temperature activity for the gas-phase oxidation of alcohols. Such promotion effect has also been reported with the partial coverage of Au with CeO_2 [19] and TiO_2 [19,20] or Pt with FeO_x [21,22] catalysts.

3.2. *Synergistic effect for the active NiO@Au ensembles: O_2-TPD and in situ DRIFTS studies*

Two mechanisms of alcohol oxidation have been proposed: classical catalytic dehydrogenation and oxidative

Table 1
Gas-phase selective oxidation of benzyl alcohol catalyzed by the various pre-activated catalysts with only Au or NiO particles, or NiO@Au-NPs ensembles. Au loading: 4 wt%, NiO loading: 4 wt%.[a]

Catalyst	Particle size (nm)		Temperature (°C)		Conv. (%)	Sel. (%)
	Au	NiO	Calcination	Reaction		
Au-4/Ni-fiber-300	25	5	300	280	99	99
Ni-fiber	–	–	300	280	<2	99
Au-4/Ni-fiber-W-300[b]	25	–	300	280	39	99
NiO-4/Ni-fiber-300[c]	–	6	300	280	5	99
NiO-4@Au-4/Ni-fiber-W-300[c]	25	5	300	280	94	99
Au-4/Ti-fiber-300	27	–	300	280	8	99
NiO-4/Ti-fiber-300[c]	–	6	300	280	4	99
NiO-4@Au-4/Ti-fiber-300[c]	26	5	300	280	95	98
Au-4@NiO/Ni-fiber-C-300	26	–	300	280	39	99
Au-4/SS-fiber-300[c,d]	23	–	300	280	17	99
NiO-4@Au-4/SS-fiber-300[c,d]	23	5	300	280	89	99

[a] All catalyst samples were prepared similarly to the Au-4/Ni-fiber-300 and were pre-activated (*i.e.*, catalysts underwent gas-phase selective oxidation of benzyl alcohol at 380 °C for 1 h using O_2/ol = 0.6 and WHSV = 20 h^{-1}) and then evaluated at the specified temperature while keeping the other reaction parameters unchanged.
[b] The freshly prepared Au-4/Ni-fiber was washed by deionized water to remove $NiCl_2$ completely ($AgNO_3$ test).
[c] NiO doping: The Ni-fiber, Au-4/Ni-fiber-W-300, Ti-fiber, Au-4/Ti-fiber-300, and Au-4/SS-fiber-300 were impregnated with aqueous $Ni(NO_3)_2$ solution followed by calcination at 300 °C.
[d] SS-fiber: Stainless steel 316L fiber.

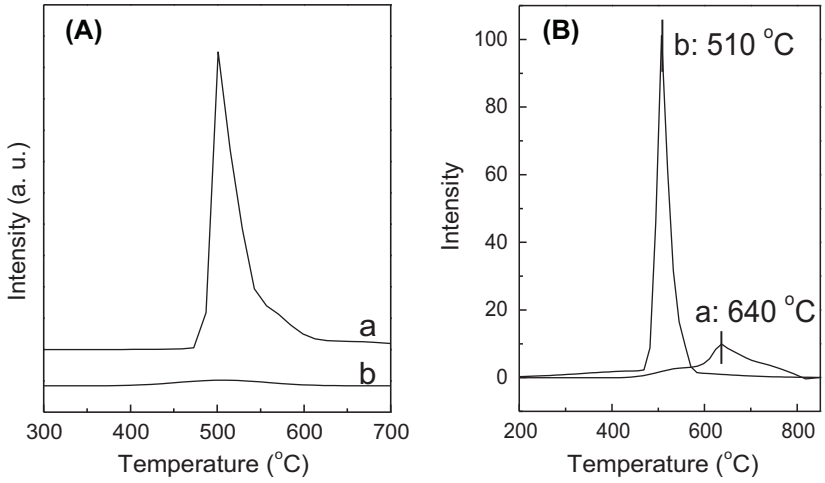

Fig. 3. The O_2-TPD profiles of several catalyst samples. (A) The O_2-TPD over the pre-activated Au-4/Ni-fiebr-300 after the gas-phase oxidation of benzyl alcohol in the presence (a) and absence (b) of O_2 for 0.5 h; (B) The O_2-TPD profiles of the pre-activated contrastive catalysts of (a) Au-4/Ti-fiber-300 and (b) NiO-4@Au-4/Ti-fiber-300. Reaction conditions: reaction temperature = 280 °C, O_2/ol = 0.6 and WHSV of 20 h^{-1}. Pre-activation conditions: same as in Fig. 1.

dehydrogenation [37]. In general, the selective oxidation of alcohols by O_2 over copper-based catalysts proceeds as follows [38]: Copper(I) oxide catalyzed alcohol dehydrogenation takes place first to form surface Cu_2O–H hydride species and alcoholates, which are subsequently decomposed into aldehydes, then the oxygen accepts the hydrogen of the hybrid by releasing the free active Cu_2O sites. Over the K–Cu–TiO_2 [34] and Au/Cu-fiber [35] catalysts, the catalytic dehydrogenation of benzyl alcohol could give a conversion of 7–8% without addition of oxygen at around 220 °C. However, the pre-activated Au-4/Ni-fiber-300 could provide a very high benzyl alcohol conversion of 99% at 280 °C with the presence of oxygen, while after switching off O_2, the benzyl alcohol conversion decreased dramatically to <1% in a few minutes (Fig. S8). The above results indicate a feasibility of the direct oxidation-dehydrogenation route for the target reaction over our Au/Ni-fiber catalyst. If so, the adsorbed oxygen species should be generated on the working catalyst surface, which are active for abstracting the hydrogen of the alcohol molecule.

To verify, TPD was used to get insight into the synergistic effect of NiO@Au ensembles anchored on Ni- or Ti-fiber surface. Fig. 3A shows the TPD signals of the pre-activated Au-4/Ni-fiber-300 catalyst after benzyl alcohol oxidation with and without adding O_2. Upon adding O_2 on the catalyst, a strong O_2 desorption signal at a maximum of ~510 °C was observed while almost completely disappeared after reacting with benzyl alcohol alone for a half hour. Additionally, only a small O_2-TPD signal at 640 °C over the Au-4/Ti-fiber-300 catalyst (Fig. 3B-a) was observed, while a strong signal was delivered at 510 °C over the pre-activated NiO-4@Au-4/Ti-fiber-300 (Fig. 3B-b). The previous results showed that all the pre-activated Au/Ni-fiber-300 catalysts with various Au-loading between 1 and 5 wt% show a single O_2 desorption signal at ~510 °C while the signal intensity increases along with the Au-loading [18]. The benzyl alcohol conversion plotted *vs.* area ratio of TPD signals illustrates a linear correlation [18]. Similar promotion effect of the post NiO-doping on the Au-4/SS-fiber-300 catalyst was also observed (Fig. S9 and Table 1). One thus can say that, on the NiO@Au ensembles, a kind of desorpable surface-active-oxygen species might be produced steadily from O_2 molecules and then would be consumed by alcohol molecules under the reaction conditions.

In situ DRIFTS experiments using ethanol as probe molecule were performed to check the activity and selectivity of the desorpable oxygen species identified above. Fig. 4A shows the temperature-programmed DRIFTS spectra for the pre-activated Au-4/Ni-fiber-300 catalyst with exposure to static ethanol gas. At 50 °C, an apparent band at 1060 cm^{-1} (ν_{C-OH}) assigned to gaseous ethanol was observed only, indicating that no any reaction occurred between ethanol and the catalyst surface. With increasing the temperature, a new band at 1700–1750 cm^{-1} ($\nu_{C=O}$) assigned to gaseous acetaldehyde appeared and got the climax at 200 °C while

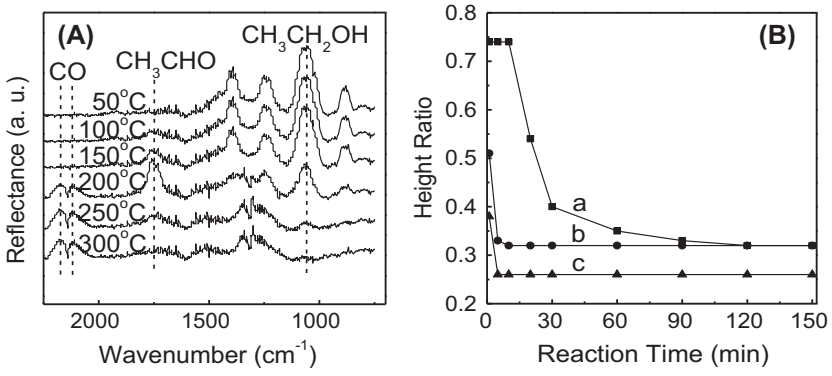

Fig. 4. (A) *In situ* DRIFTS spectra of the pre-activated Au-4/Ni-fiber-300 after exposure to static ethanol/helium mixture at programmed temperature from 50 to 300 °C. Helium flow of 30 mL/min was switched to pass through a vapor saturator with ethanol that immersed in a water bath (25 °C) for ethanol feeding. (B) The IR signal intensity ratio of the peak at 1720 cm^{-1} (CH_3CHO) to the one at 1060 cm^{-1} (C_2H_5OH) as a function of reaction time at 200 °C in the DRIFTS reactor cell (continuously filling with ethanol saturated (at 25 °C) helium) with (a) the pre-activated Au-4/Ni-fiber-300, (b) fresh Au-4/Ni-fiber-W-300, and (c) pre-activated NiO-4/Ni-fiber-300.

the ethanol ν_{C-OH} band decreased gradually and almost disappeared at 300 °C. In this course, the formation of gaseous CO and CO_2 (not shown) occurred only at and above 200 °C and increased with temperature, due to the deep oxidation of ethanol. Based on the above results in Fig. 4A, the catalytic dehydrogenation route could be ruled out, considering the nonlinear relationship of the acetaldehyde formation against the reaction temperature together with the observation of overoxidation of ethanol. In other words, the working catalyst indeed could supply a large amount of O atoms which showed excellent low-temperature activity and good selectivity for abstracting H atom from OH group of ethanol. This finding is consistent with the TPD results corroborating the fact that the oxidation of alcohols over our Au/Ni-fiber catalyst follows the oxidative dehydrogenation pathway.

Subsequently, the pre-activated Au-4/Ni-fiber-300, fresh Au-4/Ni-fiber-W-300 and pre-activated NiO-4/Ni-fiber-300 were continuously purged by ethanol/helium at 200 °C. The ethanol conversion is represented by the height ratio of the peak at 1720 cm^{-1} ($\nu_{C=O}$) to the peak at 1060 cm^{-1} (ν_{C-OH}). Interestingly, the pre-activated Au-4/Ni-fiber-300 offered the highest ethanol conversion (height ratio of 0.74) that remained for 10 min and decreased progressively along with the *in situ* reaction (Fig. 4B-a). It should be noted that there is a final height ratio of 0.32, indicating the active oxygen was used up. For the fresh Au-4/Ni-fiber-W-300, there was a high starting conversion (height ratio of 0.51), which may be caused by the surface-active-oxygen species introduced during the calcination process (Fig. 4B-b). The conversion decreased rapidly to the final height ratio of 0.32 in 5 min, indicating the much lower amount of oxygen species than that over the pre-activated Au-4/Ni-fiber-300 catalyst. For the pre-activated NiO-4/Ni-fiber-300, the starting conversion was much lower and decreased rapidly to the height ratio of 0.26 (Fig. 4B-c). It can be inferred that a large amount of surface-active-oxygen species indeed existed over the pre-activated Au-4/Ni-fiber-300.

3.3. Identification of Ni_2O_3–Au^+ hybrid active sites

3.3.1. XPS and XANES studies

Fig. 5 shows the XPS spectra in the regions of O 1s (Fig. 5A), Ni 2p (Fig. 5B), and Au 4f (Fig. 5C) for the pre-activated Au-4/Ni-fiber-300 samples. On the highly active surface of the pre-activated Au-4/Ni-fiber-300 (working sample), as one can see from spectra (a) to (c) in Fig. 5 and Table S1, apart from Au^0 and NiO, not only a large amount of Ni_2O_3 specimens (Ni 2p: 873.7 eV; O 1s: 531.8 eV, the detailed analysis in Supporting information I) but also considerable Au^+ (Au 4f (7/2): 84.8 eV) specimens were clearly detected, with surface Au^+/Ni^{3+} ratio of 1/45. Note that the O atoms adsorbed on the Au^+ sites generally exist in the form of OH groups that provide an O 1s peak also at approximately 532 eV [39]. It has been reported that the cationic gold atoms were mostly located at the gold-support interface and the corners and steps of small Au NPs (<5 nm) [2–4,40–43]. In our case, the cationic gold atoms were more preferably located at the gold-support interface according to the unique NiO@Au ensembles nanostructure than at the corners and steps of Au particles because of the large Au particles size of 25 nm. Some works have also shown that the gold atoms at the surface-phase junction with oxides could be oxidized, most possibly to the Au^+ state [36,44].

On the surface of the working catalyst after undergoing a reaction with benzyl alcohol in the absence of O_2 for 0.5 h (called exhausted catalyst), interestingly, the O 1s peak at 531.8 eV attributed to Ni_2O_3 and the Au 4f (7/2) peak at 84.8 eV attributed to Au^+ decreased significantly while the 529.7 eV O 1s peak (lattice O of NiO) increased slightly (spectra (d)–(f) in Fig. 5, Table S1). The Au 4f (7/2) peak area for Au^+ was reduced from 32 to 2%, and the Ni 2p peak area for Ni_2O_3 from 42 to 32%, which nearly stoichiometrically agrees with the reduction of the O 1s peak for Ni_2O_3 (Supporting information III and Table S1), while the NiO surface content increased from 58 to 68% (spectra (b) and (e) in Fig. 5 and Table S1). Subsequently, after the exhausted catalyst reacting with benzyl alcohol by re-feeding O_2 at 280 °C, Au^+ and Ni_2O_3 surface content both recovered to the previous level with Au^+ content of 31% and Ni_2O_3 content of 43% (spectra (g)–(i) in Fig. 5 and Table S1).

As a sensitive technology to probe the local geometry and identify the oxidative states of metallic particles [45–47], XANES was employed to further clarify the evolution behavior of Au^+ and Ni_2O_3 as shown in Fig. 6. The working catalyst showed a similar XANES with the reported mixture of Au^+ complexes and Au^0 particles (Fig. 6A-a) [45], clearly indicating the existence of Au^+. After undergoing the reaction for 0.5 h with only benzyl alcohol in the absence of O_2, the whiteline intensity of Au L^{III} over the exhausted catalyst decreased, indicating that Au^+ content reduced (Fig. 6A-b). Interestingly, after re-feeding O_2 to the exhausted catalyst, the whiteline intensity increased again to the previous level of the working catalyst, indicating that the Au^+ ions are regenerated with the similar content to that of the working catalyst (Fig. 6A-c). Additionally, the same trend was also observed in the changes of Au–O coordination (Fig. 6B). The working catalyst showed an Au–O coordination at a distance of 1.7 Å (Fig. 6B-a), similar distance with that for the catalysts reported elsewhere [45], while over the exhausted catalyst, the Au–O coordination almost disappeared (Fig. 6B-b). However, after re-feeding O_2 into the reaction stream, the Au-O coordination increased likewise to the working catalyst level (Fig. 6B-c). For the Ni_2O_3, the XANES is not as sensitive as the XPS in tracking the changes of Ni_2O_3 content in the above cases, since the existence of the Ni-fiber support leads to a very low Ni_2O_3/Ni^0 molar ratio. Even so, the high–low–high changes of whiteline intensity

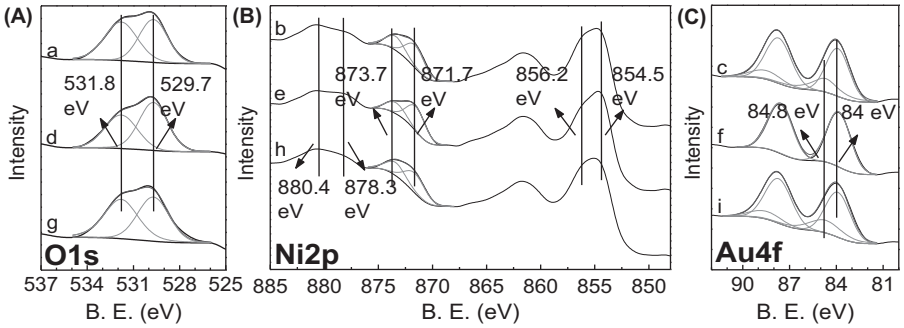

Fig. 5. XPS spectra in O 1s (A), Ni 2p (B), and Au 4f (C) regions on the catalyst surfaces. (a–c) The pre-activated (called working sample) Au-4/Ni-fiber-300; (d–f) The pre-activated Au-4/Ni-fiebr-300 experienced the gas-phase oxidation of benzyl alcohol in the absence of O_2 280 °C for 0.5 h (called exhausted sample); (g–i) The exhausted catalyst catalyzed benzyl alcohol by re-feeding O_2 (called re-activated sample) at 280 °C.

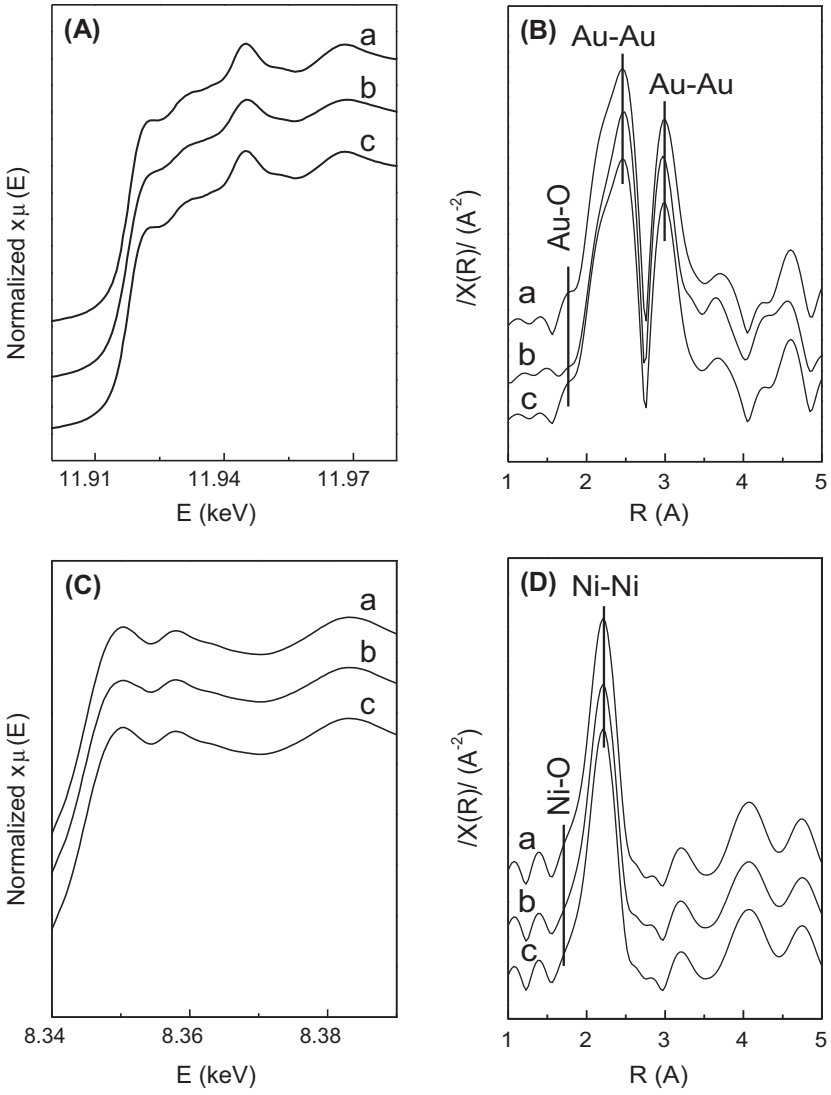

Fig. 6. Au L^{III}-edge (A) and Ni K-edge (C) XANES and modulus of the Fourier-transform Au L^{III}-edge (B) and Ni K-edge (D) signal of the samples same as in Fig. 5: (a) the working sample; (b) the exhausted catalyst; (c) the re-activated sample.

at the Ni K edge and Ni–O coordination could still be distinguished (Fig. 6C and D). Similarly, the absorption intensity at 8350 eV for the exhausted catalyst was slightly lower than that for the working one, and subsequently could retrieve to the previous level of the working catalyst by re-feeding O_2 into the reaction stream. As expected, similar evolution behaviors of XANES for both Au and Ni were also observed for NiO-4@Au-4/Ti-fiber-300 in the reaction processes with–without–with O_2 (Fig. S10). Combining with the XPS results, it could infer that the high–low–high change of the absorption intensity at 8350 eV can be assigned to the high–low–high change of Ni_2O_3 content (Supporting information IV). Furthermore, the first coordination shell was fitted and the structural parameters are summarized in Table 2. Likewise, during the with–without–with O_2 processes, the fitted coordination numbers (CN) of Au–O and Ni–O pairs exhibited the similar high–low–high change with the results from the XPS and whiteline intensity of Au L^{III} and Ni K edges (Figs. 5 and 6 and Table S1).

3.3.2. *Why Ni_2O_3–Au^+ hybrid active sites?*

Along with the high–low–high surface concentration of Ni_2O_3 and especially Au^+ (Figs. 5 and 6 and Table S1), similar evolution behavior for the benzyl alcohol conversion was also observed. Over the pre-activated Au-4/Ni-fiber-300, the benzyl alcohol conversion of 99% was obtained at 280 °C with O_2 feeding. Meanwhile, the high surface concentrations of Au^+ and Ni^{3+} were determined to be 32 and 42% (Table S1). After undergoing the reaction with benzyl alcohol alone by switching off O_2 feeding at 280 °C for 0.5 h, the benzyl alcohol conversion was decreased to an extremely low level of <1% (Fig. S8), accompanied by almost disappearance of Au^+ together with a clear reduction of Ni_2O_3 from 42 to 32% (Fig. 5 and Table S1). As the above exhausted catalyst was reacted with benzyl alcohol by re-feeding O_2 at 280 °C for 0.5 h, not only the benzyl alcohol conversion was retrieved to 95% but also the Au^+ and Ni_2O_3 surface concentrations got back to the comparable level of the pristine reactive surface (Table S1). Clearly, the high–low–high surface contents of Au^+ together with Ni_2O_3 but not NiO were associated with a parallel high–low–high change of benzyl alcohol conversion in the with–without–with O_2 processes.

Especially, the change of Au^+ surface content, in the with–without–with O_2 processes, should be noted. With the sharp high–low–high behavior of benzyl alcohol conversion (99% *vs.* 1% *vs.* 95%), the Au^+ surface content was also showed a sharp high–low–high change (32% *vs.* 2% *vs.* 31%). This good correlation between Au^+ content and conversion definitely indicated that Au^+

Table 2
XANES fit parameters for the different samples of the pre-activated Au-4/Ni-fiber-300 from first-shell analysis of the Au L^{III} and Ni K edges.[a]

Samples[b]	Shell	CN (±10%)	R (Å) (±0.02 Å)	$\Delta\sigma^2$ ($\times10^{-3}$ Å^2)
Sample 1 (working)	Au–Au	11.3–11.4	2.85	3.5
	Au–O	0.4–0.5	1.98	8
	Ni–Ni	11.4–11.5	2.49	3.1
	Ni–O	0.4	2.06	7
Sample 2 (exhausted)	Au–Au	11.6–11.8	2.85	3.2
	Au–O[c]	0.0–0.1	1.98	0.8
	Ni–Ni	11.4–11.5	2.49	3.1
	Ni–O	0.3	2.06	6.3
Sample 3 (re-activated)	Au–Au	11.3–11.4	2.85	3.4
	Au–O	0.4–0.5	1.98	8.1
	Ni–Ni	11.4–11.5	2.49	3.2
	Ni–O	0.4	2.06	7

[a] CN, coordination number; R, distance between absorber and backscatterer atoms; $\Delta\sigma^2$, Debye–Waller factor.
[b] The samples are the same ones as in Fig. 6.
[c] This contribution is too small to allow for a confident assignment. It was included to make the overall fitting complete.

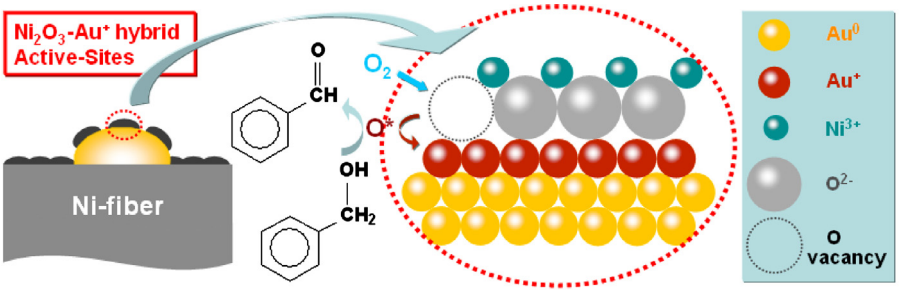

Scheme 1. Structural scheme of the hybrid active site of Ni_2O_3–Au^+ on NiO@Au ensembles over the pre-activated Au-4/Ni-fiber-300.

governed the alcohol oxidation. Whereas the surface Ni_2O_3 exhibited a similar high–low–high trend (*e.g.*, 42% *vs.* 32% *vs.* 43%), the change is smaller compared with the benzyl alcohol conversion and Au^+ surface content. In the case of without O_2 feeding, the catalyst showed a surface Ni_2O_3 concentration of 32% but delivered a conversion of <1% with almost complete disappearance of Au^+. It could thus infer that only Ni_2O_3 in the absence of Au^+ is inactive for the alcohol oxidation and O species adsorbed on the Au^+ are active for the low-temperature selective oxidation of alcohols *via* the direct-oxidation dehydrogenation route [37]. The above results indicated that the Au^+ served as main active species for the alcohol oxidation, and Ni_2O_3 as an assistant for the oxidation. It has been reported that the Ni_2O_3 specimens could supply active oxygen species, acting as an oxygen buffer by releasing-uptaking oxygen through redox processes [14,32,48].

Since surface Au^+ content changed in parallel with the Ni_2O_3 content in the experimental operation with–without–with O_2 feeding, there should have some kind of certain interaction between Au^+ and Ni_2O_3. Some reported findings [3,23,36,44] indicated that cationic gold could be stabilized by metal oxides. For example, CeO_2 is reported to be able to stabilize cationic gold (Au^+ and Au^{3+}) [36], even at the temperature of 300–400 °C for water-gas shift reaction. Additionally, TiO_2 is also reported to be able to stabilize cationic gold in the oxidation reactions, such as CO oxidation [3,23,44]. Besides the stabilization of cationic gold by metal oxides, the cationic Pt also could be stabilized by metal oxides, such as $Pt^{\delta+}$ by CeO_2 [36]. In accordance, from the reported and our results, the stabilization of the cationic noble metal by metal oxides, especially the transition metal oxides, seems to be a wide and interesting phenomenon.

From above results and discussion, hybrid active site of Ni_2O_3–Au^+ is tentatively proposed as illustrated in Scheme 1. The oxygen atoms from O_2 in the gas phase are adsorbed on the oxygen vacancy of Ni_2O_3 and then spillover to the Au^+ cations to selectively and actively react with alcohols there. Besides activating and transferring O_2 [14,32,48], Ni_2O_3 specimens at high surface concentration might facilitate formation of Au^+ cations and stabilize them [3,23,36,44].

3.4. Ni_2O_3–Au^+ hybrid active sites: evidence from catalyst deactivation

In the life-time test, benzyl alcohol conversion steadily remained at 90% [31]. After benzyl alcohol conversion decreased to 85%, the Au-4/Ni-fiber-300 was measured by XRD every 2 h. After 8 h, the benzyl alcohol decreased to 14%. Fig. 7 shows the

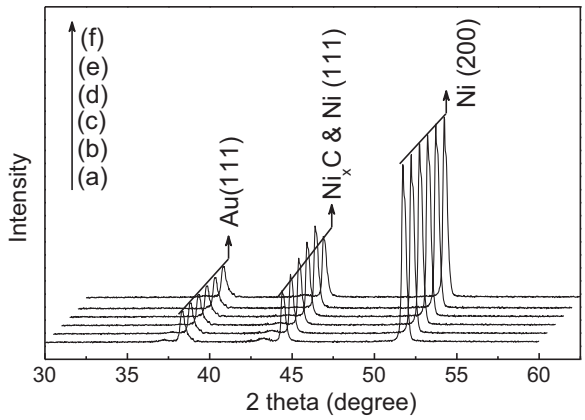

Fig. 7. The XRD patterns of the Au-4/Ni-fiber-300 catalyst samples: (a) working, (b-e) deactivated: collected every 2 h, and (f) regenerated samples. Pre-activation conditions: same as in Fig. 1. Regeneration conditions: the deactivated sample was treated in air at 380 °C for 2 h.

XRD patterns of the working, deactivated and regenerated Au-4/Ni-fiber-300 samples. It is clear that the characteristic diffraction peak at 44° increased progressively along with the time during the deactivation process, which indicates that the parent Ni_xC phase was definitely formed in the deactivated sample. The (Ni(1 1 1) + Ni_xC)/Au(1 1 1) ratio increased from 1.5 for the working sample (Pattern a in Fig. 7) to 2.4 for the deactivated sample (Pattern e in Fig. 7) while the benzyl alcohol conversion decreased from 98 to 14% (Fig. 7 and Table S2). After heating the deactivated catalyst at 380 °C in air for 2 h, the Ni_xC was removed mostly with the (Ni(1 1 1) + Ni_xC)/Au(1 1 1) ratio down to 1.6 (Pattern f in Fig. 7) while the Au particle size remained unchanged. Over such regenerated catalyst, the benzyl alcohol conversion recovered almost to the original level of 94% at 280 °C. Therefore, transformation of NiO into the Ni_xC is the main cause for the catalyst deactivation, likely switching off O_2 activation/transportation path from the Ni_2O_3 (oxygen activation center) to Au^+ (reaction center).

The working and deactivated samples were further investigated by XPS, and the relative portions of NiO/Ni_2O_3 and Au^+/Au^0 were calculated and summarized in Table S3. The Ni^{3+}/Ni^{2+} ratio in the deactivated catalyst was higher than that in the working sample, while the Au^+/Au^0 ratio, in a contrast, decreased after the catalyst deactivation. Most probably, the Ni_xC compounds cut off O_2 activation/transportation path from the Ni_2O_3 to Au^+ while causing the oxygen over-accumulation. As a result, the Ni^{3+}/Ni^{2+} ratio was increased from 42/58 on the working surface to 71/29 on the deactivated sample surface (Table S3). For the same reason, the Au^+/Au^0 ratio was decreased sharply from 32/68 on the working surface to 9/91 on the deactivated one.

4. Conclusions

The interesting date-cake-like active NiO@Au ensembles with special structure of partial coverage of large Au particles with small NiO segments are identified to be indispensable to achieve the low-temperature gas-phase oxidation of alcohols. Over such ensembles, the active-sites of Ni_2O_3–Au^+ are defined and special synergistic effect exists between Ni_2O_3 and Au^+. The Ni_2O_3 specimens not only can increase and stabilize Au^+ but also act as the activation center for O_2, and Au^+ acts as the reaction center for alcohol oxidation. The Ni_2O_3–Au^+ hybrid active sites work in the way that the oxygen molecules are adsorbed and dissociated on the oxygen vacancy of Ni_2O_3 (oxygen activation center) and then spillover to the Au^+ cations to highly selectively and actively oxidize alcohols there while releasing oxygen vacancy for next catalytic cycle. The Ni_xC compounds are found to be formed along with the reaction and can interrupt the O_2 activation/transportation path from the Ni_2O_3 to Au^+ cations thereby leading to catalyst deactivation with significant reduction of surface concentration of Au^+–Ni_2O_3 hybrid active sites.

Acknowledgments

This work was funded by the NSF of China (21076083, 20973063, 21273075), the “973 program” (2011CB201403) from the MOST of China, the Fundamental Research Funds for the Central Universities, the Shanghai Rising-Star Program (10HQ1400800), the Specialized Research Fund for the Doctoral Program of Higher Education (20090076110006), and the Shanghai Leading Academic Discipline Project (B409). We thank the Electron Spectroscope Center of the East China Normal University for assistance with TEM measurements.

Appendix A. Supplementary data

Supplementary data associated with this article can be found, in the online version, at http://dx.doi.org/10.1016/j.apcatb.2013.04.015.

References

[1] M. Haruta, N. Yamada, T. Kobayashi, S. Iijima, Journal of Catalysis 115 (1989) 301.
[2] G.C. Bond, D.T. Thompson, Catalysis Reviews – Science and Engineering 41 (1999) 319.
[3] A.S.K. Hashmi, G.J. Hutchings, Angewandte Chemie International Edition 45 (2006) 7896.
[4] B.K. Min, C.M. Friend, Chemical Reviews 107 (2007) 2709.
[5] G.J. Hutchings, Dalton Transactions (2008) 5523.
[6] M.S. Chen, D.G. Goodman, Science 306 (2004) 252.
[7] R. Meyer, C. Lemire, S.K. Shaikhutdinov, H.-J. Freund, Gold Bulletin 37 (2004) 72.
[8] A.A. Herzing, C.J. Kiely, A.F. Carley, P. Landon, G.J. Hutchings, Science 321 (2008) 1331.
[9] J.C. Fierro-Gonzalez, B.C. Gates, Chemical Society Reviews 37 (2008) 2127.
[10] M. Comotti, W.C. Li, B. Spliethoff, F. Schüth, Journal of the American Chemical Society 128 (2006) 917.
[11] P.X. Huang, F. Wu, B.L. Zhu, X.P. Gao, H.Y. Zhu, T.Y. Yan, W.P. Huang, S.H. Wu, D.Y. Song, Journal of Physical Chemistry B 109 (2005) 19169.
[12] J. Li, N. Ta, Y. Li, W.J. Shen, Chinese Journal of Catalysis 29 (2008) 823.
[13] R. Si, M. Flytzani-Stephanopoulos, Angewandte Chemie International Edition 47 (2008) 2884.
[14] J. Guzman, S. Carrettin, A. Corma, Journal of the American Chemical Society 127 (2005) 3286.
[15] A. Abad, P. Concepción, A. Corma, H. García, Angewandte Chemie International Edition 44 (2005) 4066.
[16] S. Biella, M. Rossi, Chemical Communications 3 (2003) 378.
[17] C.D. Pina, E. Falleta, M. Rossi, Journal of Catalysis 260 (2008) 384.
[18] G.F. Zhao, H.Y. Hu, M.M. Deng, Y. Lu, Chemical Communications 47 (2011) 9642.
[19] J.A. Rodriguez, S. Ma, P. Liu, J. Hrbek, J. Evans, M. Pérez, Science 318 (2007) 1757.
[20] T. Fujitani, I. Nakamura, T. Akita, M. Okumura, M. Haruta, Angewandte Chemie International Edition 48 (2009) 9515.
[21] S. Shaikhutdinov, Y.N. Sun, Z.H. Qin, M. Lewandowski, E. Carrasco, M. Sterrer, H.J. Freund, Journal of Catalysis 266 (2009) 359.
[22] Q. Fu, W.X. Li, Y. Yao, H. Liu, H.Y. Su, D. Ma, X.K. Gu, L. Chen, Z. Wang, B. Wang, X. Bao, Science 328 (2010) 1141.
[23] G.C. Bond, D.T. Thompson, Gold Bulletin 33 (2000) 41.
[24] F. Maroun, F. Ozanam, O.M. Magnussen, R.J. Behm, Science 293 (2001) 1811.
[25] M.S. Chen, D.W. Goodman, Science 310 (2005) 291.
[26] F. Besenbacher, I. Chorkendorff, B.S. Clausen, B. Hammer, A.M. Molenbroek, J.K. Nørskov, I. Stensgaard, Science 279 (1998) 1913.
[27] X. Tan, G.W. Yang, Journal of Alloys and Compounds 467 (2009) 428.
[28] D.I. Enache, J.K. Edwards, P. Landon, B. Solsna-Espriu, A.F. Carely, A.A. Herzing, M. Watanabe, C.J. Kiely, D.W. Knight, G.J. Hutchings, Science 311 (2006) 362.
[29] S.H. Zhou, H.F. Yin, V. Schwartz, Z.L. Wu, D.R. Mullins, B. Eichhorn, S.H. Overbury, S. Dai, ChemPhysChem 9 (2008) 2475.
[30] M. Haruta, Chemical Record 3 (2003) 75.
[31] G.F. Zhao, Y.F. Jiang, M.M. Deng, H.Y. Hu, Q.S. Xue, Y. Lu, Journal of Catalysis 301 (2013) 46.
[32] M.M. Deng, G.F. Zhao, Q.S. Xue, L. Chen, Y. Lu, Applied Catalysis B 99 (2010) 222.
[33] A. Villa, G.M. Veith, D. Ferri, A. Weidenkaff, K.A. Perry, S. Campisia, L. Prati, Catalysis Science & Technology 3 (2013) 394.
[34] J. Fan, Y.H. Dai, Y.L. Li, N.F. Zheng, J.F. Guo, X.Q. Yan, G.D. Stucky, Journal of the American Chemical Society 131 (2009) 15568.
[35] G.F. Zhao, H.Y. Hu, M.M. Deng, M. Ling, Y. Lu, Green Chemistry 13 (2011) 55.
[36] Q. Fu, H. Saltsburg, M. Flytzani-Stephanopoulos, Science 301 (2003) 935.
[37] T. Mallat, A. Baiker, Chemical Reviews 104 (2004) 3037.
[38] V.Z. Fridman, A.A. Davydov, K. Titievsky, Journal of Catalysis 222 (2004) 545.
[39] L.C. Wang, L. He, Q. Liu, Y.M. Liu, M. Chen, Y. Cao, H.Y. He, K.N. Fan, Applied Catalysis A 344 (2008) 150.
[40] A. Corma, H. Garcia, Chemical Society Reviews 37 (2008) 2096.
[41] L.D. Burke, Gold Bulletin 31 (1998) 39.
[42] R.J. Davis, Science 301 (2003) 926.
[43] J. Guzman, B.C. Gates, Angewandte Chemie International Edition 42 (2003) 690.
[44] I.N. Remediakis, N. Lopez, J.K. Nøskov, Angewandte Chemie International Edition 44 (2005) 1824.
[45] J. Guzman, B.C. Gates, Journal of the American Chemical Society 126 (2004) 2672.
[46] M.K. Oudenhuijzen, J.A. van Bokhoven, J.T. Miller, D.E. Ramaker, D.C. Koningsberger, Journal of the American Chemical Society 127 (2005) 1530.
[47] J.A. van Bokhoven, C. Louis, J.T. Miller, M. Tromp, O.V. Safonova, P. Glatzel, Angewandte Chemie International Edition 45 (2006) 4651.
[48] A. Trovarelli, Catalysis Reviews – Science and Engineering 38 (1996) 439.